# EVALUATION OF SEGMENTATION PROCEDURES USING X-RAY COMPUTED MICROTOMOGRAPHY IMAGES OF COQUINAS FROM MORRO DO CHAVES FORMATION – NE BRAZIL

**Fernanda O. Hoerlle**
fernandahoerlle@petroleo.ufrj.br
**William G. A. L. Silva**
wmgodoy@petroleo.ufrj.br
**Edmilson H. Rios**
edmilson@petroleo.ufrj.br
**Thaís M. G. Silveira**
thais@petroleo.ufrj.br
**Paulo Couto**
pcouto@petroleo.ufrj.br
**José L. D. Alves**
jalves@lamce.coppe.ufrj.br
**Maira C. O. Lima**
mairalimarj@gmail.com
Programa de Engenharia Civil, COPPE/Universidade Federal do Rio de Janeiro
Cidade Universitária, P.O. Box 68548, Rio de Janeiro, Brazil
**Leonardo Borghi**
lborghi@geologia.ufrj.br
Laboratório de Geologia Sedimentar (Lagesed), Instituto de Geociências, Universidade Federal do Rio de Janeiro
Av. Athos da Silveira Ramos, 274, CCMN-IGEO-Departamento de Geologia, Bloco G
**Patrick W. M. Corbett**
P.W.M.Corbett@hw.ac.uk
Heriot-Watt University
Edinburgh Campus, Edinburgh EH14 4AS, United Kingdom

***Abstract.*** *In recent years, the petroleum industry started to increase the use of digital image techniques, as X-ray computed microtomography (μCT), aiming the characterization of reservoir rocks. A frequent challenge is to determine the threshold value that binarizes the rock image into pore and matrix (solid phase). In this study, three coquinas samples from Morro do Chaves Formation, which are considered an analogue to the Pre-salt reservoirs, were analyzed aiming the quantification of their porosity through μCT images. This work compares manual and different automated segmentation methods using the μCT images with two different pixel sizes, 18μm and 10μm. The automated segmentation methods have well-*

*defined computational algorithms that automatically select the threshold value and isolate the porous space and the matrix of the rock. The codes used were clustering-based, minimum error-based and local-based methods as well as an active contour without edges procedure. The porosity results of different segmentation techniques were compared with the one obtained with a helium porosimeter, which is the industry standard procedure to measure the porosity of rocks. Comparing all the data it was possible to define the best image resolution and segmentation technique for these coquina rocks.*

**Keywords:** Binarization, Carbonate rocks, Digital petrophysics, Porosity, Digital image techniques

## 1. INTRODUCTION

In recent years, the petroleum industry started to increase the use of digital image techniques, like the X-ray computed microtomography (µCT), aiming the characterization of reservoir rocks. As a non-destructive technique, it allows 3D visualization of the internal structure of porous rocks .The porosity and pore connectivity are important rock properties and their quantitative characterization is fundamental for understanding their hydraulic behavior.

As a result of the µCT acquisition, gray-scale images of the plugs are obtained, which represent cross-sections of these samples. These cross sections are stacked to form a 3D image of the sample. According to Neto et al. (2011) and Dias et al. (2016), the greatest limitation of the technique is the image resolution and the quality of computational processing techniques. Depending on the resolution and pixel size, minor minerals and pores are not visualized, which may affect the results. In this study, the pixel sizes are approximately 20µm and 10µm, which means that a significant amount of pores may not be detected in the final porosity study due to the spatial resolution obtained with the mentioned pixel sizes. This study will investigate how the different pixel sizes affect the calculation of the total porosity.

To separate the rock pore space from its matrix (solid phase), the µCT images must be segmented. Segmentation is the process of converting a grayscale or color image to a binary image, by identifying two populations, based on the intensity of its values obtained with the tomographic acquisition (Al-Raoush & Willson, 2005). In the studies involving the analysis of rocks and their respective porous systems, for example, these two populations refer to the porous phase and the solid phase, being possible to differentiate the pores from the bulk rock. These phases are identified due to the different absorption properties of the materials and to the local attenuation coefficients (Wildenscheld et al., 2002).

Although there are several segmentation methods and extensive efforts and resources to improve the interpretation of µCT images, it lacks in the literature research on threshold methods in carbonate rocks, which are complex porous media (Corbett & Borghi, 2013). The objective of this work is to compare manual and different automated segmentation methods using the µCT images of three coquinas samples with two different resolutions. In this way, it is determined if there is a specific imaging technique or method that is capable to evaluate these carbonate rocks and how the pixel size of the µCT impacts the results. The porosity obtained by the segmentation of the µCT images is compared with the measures acquired by a helium porosimeter equipment, which is the industry standard procedure to measure the porosity of rocks (Lucia, 2007). Comparing all the data is possible to define the best segmentation technique to calculate the coquinas' porosity among those that were chosen.

The coquinas (shelly limestones) of the Morro do Chaves Formation are widely used in laboratories across Brazil as analogues for the Pre-salt reservoirs (Corbett & Borghi, 2013). In some studies, a combination of manual and automated techniques has been used in the segmentation process (Corbett et al., 2017).

## 2. OVERVIEW OF SEGMENTATION TECHNIQUES

There are many segmentation methods in literature that can be used for rock analysis. Sezgin & Sankur (2004) studied several segmentation methods and divided them into different groups, according to the information they exploit. They were classified as: histogram shape-based, entropy-based, object attribute-based, spatial, local and clustering-based. This paper uses methods that fit in the last two groups and their algorithms will be implement with Matlab®. Besides that, it will be used the Active Contour without Edge method created by Chan & Vese (2001) and a Manual method.

### 2.1 Cluster-based methods

In the clustering-based method the µCT image, which is in gray-level colors, are clustered always in two parts, as foreground and background. The image's histogram is modeled as a mixture of two Gaussians and each peak or a lobe of the histogram is determined as one cluster (Sezgin & Sankur, 2004). It will be used three methods, which are inserted in the clustering-based methods, they are: Riddler-Calvard, Otsu and Kittler-Illingworth.

***Ridler-Calvard.***

The clustering-based method studied by Ridler & Calvard (1978), also known as Isodata, was one of the first interactive schemes based on models with two-class Gaussian distributions. Basically, this method, at a given iteration $n$, finds a threshold value called $T_n$, obtained from the mean of the object and background classes, in such a way that the iteration ends when the changes in the values of these means become small enough (Sezgin & Sankur, 2004). The presence of two main peaks in a grayscale histogram demonstrates the existence of two distinct luminance regions, one corresponding to the object and the other to the background. A great advantage of this method is that the processed image always shows itself as a white object contrasting under a black background, since different levels are established for the object and the background (Silva, 2015).

***Otsu.***

Cluster-Otsu method selects automatically a threshold value from a grey level image (Otsu, 1979). The method is based on minimizing the weighted sum of the inherent variances of two classes, the object (rock matrix) and the background (porous media), thus establishing an optimal threshold. It is important to emphasize that the minimization of the inherent variances of each class is equivalent to the maximization of the data between these classes. In addition, the best results for this method occur when the number of pixels in a class, such as that of the object, for example, approximates the number of pixels in the background (Sezgin & Sankur, 2004). An optimal threshold value is selected automatically and presents great stability, since the technique is based on the integration of the histogram, which is a global property, and not on the differentiation, which is a local property of the same (Silva, 2015).

***Kittler-Illingworth.***

The Cluster–Kittler & Illingworth is different from the other methods already mentioned since it does not use the histogram analysis as reference to select a threshold value. The method uses simple statics on the image instead and automatically selects a threshold value. It removes the equal variance assumption and, in essence, addresses a minimum error Gaussian density-fitting problem (Kittler & Illingworth, 1986; Sezgin & Sankur, 2004).

## 2.2 Local-based method

Different from the Cluster based method, in the local methods the threshold value of each pixel is adjusted and calculated to the local image characteristics. The threshold value $T\ (i,\ j)$ is a function associated to each pixel of coordinates $(i,\ j)$ or, when this is not possible, the algorithm uses a logical variable $B\ (i,\ j)$ to the separation between the object and the background. The value is determined according to local statistics as variance, range or surface-fitting parameters of the pixel zone (Sezgin & Sankur, 2004).

***Local Niblack.***

The local method proposed by Niblack (1986) uses the local variance as the evaluation parameter, based on obtaining the standard deviation $\sigma(i,j)$ and the local mean $m(i,j)$, calculated for a window of pixels Dimensions $b \times b$ (Sezgin & Sankur, 2004). The Eq. (1) used to implement the algorithm is given by:

$$T(i,j) = m(i,j) + k\sigma(i,j). \tag{1}$$

where $k$ is a set value and it is equal to 0.2 for light objects and –0.2 for dark objects. Thus, depending on the calculated value of $T(i,j)$, a given neighborhood composed of a window of $b \times b$ pixels is associated with the object or background.

## 2.3 Active Contour without Edges method

Sezgin & Sankur (2004) do not mention the method Active Contours without Edges (ACWE). It was created by Chan & Vese (2001) and will be implemented in the µCT 2D images of the studied samples. It is based on curve evolution and Mumford–Shah (Mumford & Shah, 1989 *apud* Chan & Vese, 2001) segmentation techniques. This method does the binarization according to the detection of the boundaries of the objects in a given image.

Due to the fact that the model does not have a stop edge-function, it can detect contours either with or without a gradient. For example, images with objects that have discontinuous, continuous, smooth, noise and sharp boundaries can be analyzed. And the initial image does not have to be filter or improved its quality before applying this method (Chan & Vese, 2001).

The interior contour of objects is detected from an initial curve that start anywhere in the image and contours the entire object (Chan & Vese, 2001). In this study case, the curve determines the boundary between the pore space of the rock sample and its matrix. As a result, the method gives a binarized image.

The code used in this method is analyzed in the Matlab® Program. The issue with this method is that it gives a binarized image, but it does not provide a threshold value. Therefore, it is necessary to open the segmented image in a program like Fiji® or Avizo® and do the segmentation over again, but now comparing the original image with the one segmented by the ACWE. Thus, the threshold value and the porosity of the sample can be determined.

### 2.4 Manual method

The manual segmentation is based on the evaluation of the 2D images that depends on the knowledge and interpretation of the operator, and it has no algorithm associated to it. For this reason it may be uncertain and it can present segmentation errors and bias difficult to predict and correct (Iassonov et al., 2009). Besides that, this procedure can be a time consuming activity. Therefore it is necessary to have a segmentation algorithm that does not require supervision and that give a satisfactory result when compared with experimental methods as the one measured by helium gas for porosity, or nitrogen gas for permeability. However, the manual segmentation can produce quality segmentation results if the operator is trained for it (Vidal & Soares, 2015).

## 3. MATERIALS AND INSTRUMENTATION

The studied rocks used in this work are the coquinas from Morro do Chaves Formation, located in Sergipe-Alagoas Basin, Northeast Brazil. These rocks are formed by bioclasts, mainly by lacustrine bivalves, which were transported and affected by several stages of diagenesis, which entailed a complex porous system (Corbett et al., 2016; Estrella, 2015).

Three samples of these coquinas named as MC-1, MC-2 and MC-3 are analyzed. Estrella (2015) studied the same samples, however with the name of 1-18B, 1-19B and 1-34A, respectively. The samples were plugged in cylindrical shape with approximately 3.5cm wide and 3.4cm long and the images from the µCT were obtained with two different pixel sizes, 9.97µm and approximately 18µm (Figure 1). The µCT equipment used was the SkyScan1173 from Bruker, belonging to Nuclear Instrumentation Laboratory (LIN/COPPE/UFRJ). This equipment was calibrated with a voltage of 130kV and 61µA. In order to reduce noise, a 0.5mm copper filter was added at the acquisition stage. The plugs were rotated 360º with 0.5º angular pitch. For the images of 18µm, the average time of acquisition was approximately 1 hour and 27 minutes, the reconstruction time ranged from 16 minutes to 36 minutes and it was generated between 2,179 and 2,210 sections of µCT images for each sample. In turn, the 9.97µm images had an average time of acquisition of approximately 7 hours and 30 minutes, the reconstruction time was around 7 hours and it was generated between 3,294 and 4,336 sections of µCT images for each plug (Table 1).

The µCT images will be segmented using six different methods, five of them automated and based on algorithms to calculate the threshold value. The last one is manual and depends on the operator's knowledge.

Table 1. Some parameters of µCT acquisition of the three coquinas samples from Morro do Chaves Formation, Sergipe-Alagoas basin, northeast Brazil.

| Sample | Acquisition Time (h) | Number of Sections | Reconstruction Time (h) | Pixel Size (µm) | Image Resolution (µm) |
|---|---|---|---|---|---|
| **MC-1** | 1.3706 | 2,205 | 0.6125 | 16.03 | 42.22 |
| **MC-1** | 6.7250 | 3,294 | 6.9639 | 9.97 | 26.22 |
| **MC-2** | 1.3783 | 2,179 | 0.5881 | 18.87 | 49.72 |
| **MC-2** | 8.0969 | 4,304 | 9.9061 | 9.97 | 26.22 |
| **MC-3** | 1.6611 | 2,210 | 0.2803 | 18.16 | 47.84 |
| **MC-3** | 7.7358 | 4,336 | 6.6831 | 9.97 | 26.22 |

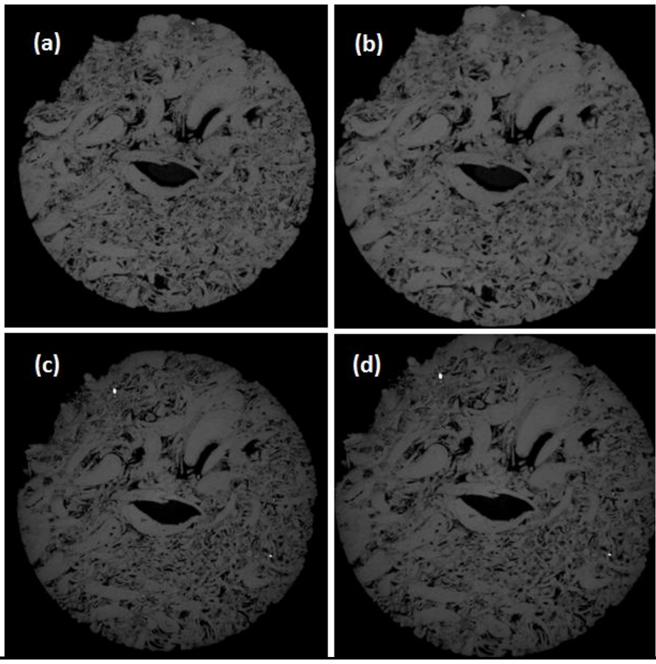


Figure 1. µCT images from plug MC-2 with pixel size of 9.97µm (a) without filter and (b) with non-local means filter; and with pixel size of 18.87µm (c) without filter and (d) with non-local means filter.

The algorithms that provided the threshold value were implemented with Matlab®. Besides the threshold value, the ACWE, Ridler-Calvard, Niblack and Otsu methods also generate a segmented image (Figure 2). Kittler-Illingworth algorithm only gives a threshold value as a result. Because the Manual method has no algorithm to run, it was analyzed exclusively with Avizo®.

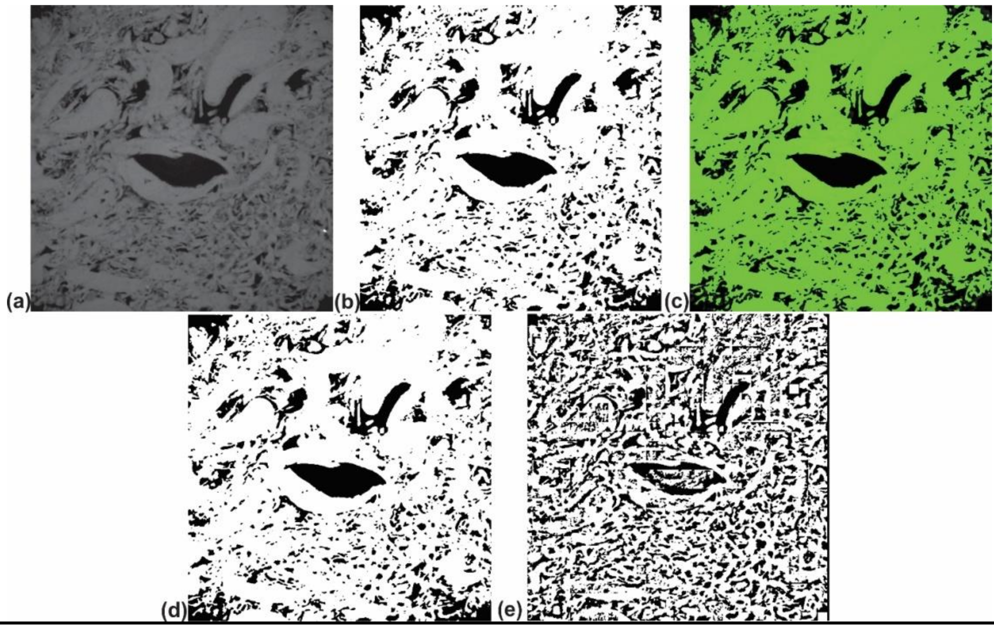


Figure 2. µCT image of a slice of sample MC-2, from Morro do Chaves Formation, with pixel size of 18.87µm (a) with non-local means filter, (b) segmented with Otsu method, (c) segmented with 12,000 interactions using the Active Contour without Edges method, (d) segmented with Ridler-Calvard method, (e) segmented with Niblack method.

The Kittler-Illingworth, Ridler-Calvard, Niblack and Otsu methods are fast to run, they take from 5 minutes to 15 minutes to give a threshold result. On the other hand, the ACWE method, which was run with 12,000 interactions, took 4 hours to 12 hours to segment the images (Figure 3). The processing depends on the computer hardware and the pixel size, images with 9.97μm take longer to analyze.

The procedure for the segmentation of the μCT images and the porosity calculation using the Manual method is the same adopted by Vidal & Soares (2015). The μCT images are divided into three phases: macro porous, micro porous and rock matrix. Hence, two threshold values are determined, one for the macroporosity and other for the microporosity. The shades of gray determine the difference between them. The macroporous are the black areas on the images and the microporous are the dark gray area surrounding the macroporous (Figure 4). The final porosity is the sum of the macroporosity and the microporosity.

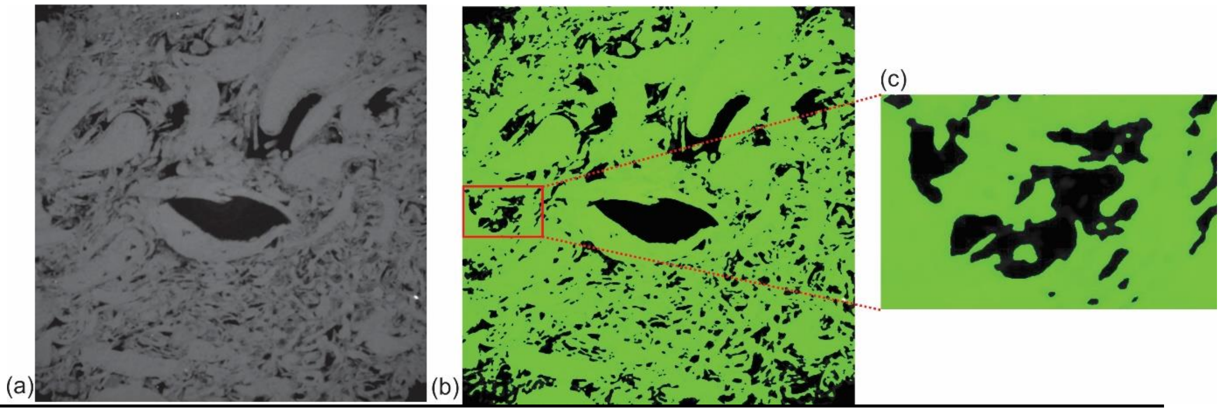


Figure 3. μCT image of plug MC-2, from Morro do Chaves Formation, with pixel size of 18.87μm (a) with non-local means filter; (b) segmented with 12,000 interactions using the Active Contour without Edges method, with a threshold value of 48; (c) zoom in a segmented region of sample MC-2. Gray and green colors represent the rock matrix and black the porous space.

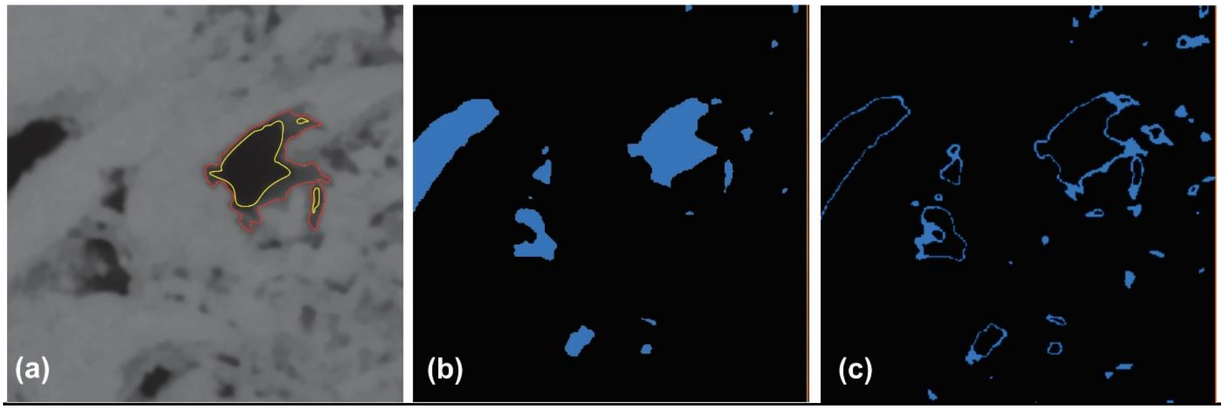


Figure 4. (a) μCT image with a specific region cropped from plug MC-2 with pixel size of 9.97μm, the area inside the yellow border is considered the macroporous, the area between the yellow and red borders is considered microporous; (b) the same region segmented with the Manual method using a threshold of 30 for the macroporous; (c) the same region segmented with the Manual method using a threshold of 46 for the microporous. Images obtained through Avizo®.

## 3.1 IMAGE PROCESSING AND ANALYSIS

It is necessary to process the μCT image before its analysis. As the first step it was used a non-local means filter, from Avizo®, to eliminate the "salt and pepper" effect of the image and to minimize any artifacts or noises due to the acquisition process (Iassonov et al., 2009). The second step was to select a region of interest (ROI) to work. The ROI correspond to a cropped region that contains only the image of the rock, excluding the exterior part correlated to the outside air and the container walls. In this way it was possible to work with different segmentation algorithms and have a reliable basis to compare them.

For Ridler-Calvard, Kittler-Illingworth, Niblack and ACWE methods it was used 2D images, because the algorithms available only read one image per time. The images chosen were the ones more representative of the sample and with fewer artifacts. For each sample were selected three μCT images, from the top, central and bottom of the plug (Figure 5). Thus, it was possible to do an arithmetic mean with the obtained threshold values to find a more representative porosity result.

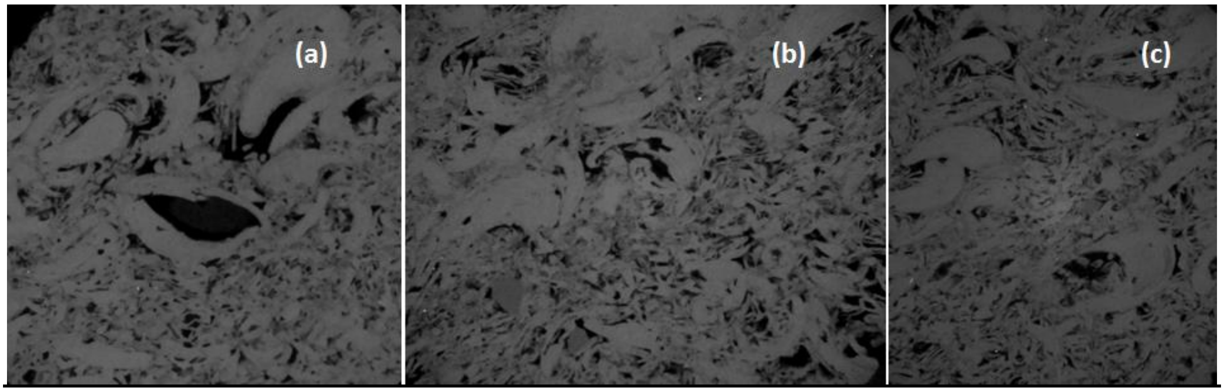


Figure 5. μCT images of the plug MC-2, from Morro do Chaves Formation, with pixel size of 9.97μm representing the (a) top, (b) central and (c) bottom regions.

The Otsu and Manual methods could be executed with the 3D images from the whole plug. However, it was also used 2D images to be able to compare their results with those acquired with the other three methods.

To obtain the porosity value of each sample, the images trimmed and filtered were evaluated on Avizo®. Each image was open in this program, the threshold value of each method was set using the *Interactive Threshold* function and the images were segmented. Using the *Material Statistics* function it was possible to quantify the pixels of the pore system and the pixels of the rock matrix. Therefore, the porosity of each sample was calculated according to the Eq. (2):

$$\Phi = \frac{nP}{nT}, \; nT = nM + nP. \tag{2}$$

where $\Phi$ is the porosity, $nP$ is the number of pixels of the pore system, $nM$ is the number of pixels if the rock matrix, and $nT$ is the total number of pixel of the image.

To conclude the comparative analyses of the study, it was determined the arithmetic mean of the three threshold values found for each image using the six segmentation methods for the three samples. The new threshold value was used to segment a volume of interest (VOI) of the whole plug. The porosity of the VOI was calculated in the same way as the individual images. The porosity found using the segmentation methods was compared with the helium porosity measured in the Weatherford DV-4000 Automated Porosimeter, at the Enhanced Oil Recovery Laboratory (LRAP/COPPE/UFRJ).

## 4. RESULTS

The µCT images of three samples from Morro do Chaves Formation, MC-1, MC-2, and MC-3 were obtained with two different resolutions and three µCT images for each sample where segmented using different algorithms. The algorithms used come from the Kittler & Illingworth (1986), Ridler & Calvard (1978), Otsu (1979), Chan & Vese (2001) with the ACWE, Niblack (1986), and Manual method (Iassonov et al., 2009; Vidal & Soares, 2015). Each method provided a threshold value for the image segmented, which are listed on Table 2.

Table 2. Threshold values for the segmentation of three images from the top (T), center (C) and bottom (B) of three plugs from Morro do Chaves Formation (MC-1, MC-2 and MC-3) using six different segmentation methods.

| **Sample** | | **Pixel Size (µm)** | **Methods – Threshold** | | | | | | |
|---|---|---|---|---|---|---|---|---|---|
| | | | Kittler-Illingworth | Ridler-Calvard | Otsu | ACWE | Niblack | Manual Porosity Macro | Manual Porosity Micro |
| **MC-1** | T | 9.97 | 73 | 60 | 73 | 60 | 60 | 38 | 55 |
| | | 16.03 | 105 | 99 | 105 | 101 | 100 | 23 | 37 |
| | C | 9.97 | 89 | 85 | 89 | 87 | 86 | 45 | 60 |
| | | 16.03 | 107 | 100 | 107 | 101 | 100 | 44 | 65 |
| | B | 9.97 | 78 | 67 | 78 | 68 | 67 | 29 | 49 |
| | | 16.03 | 90 | 78 | 90 | 79 | 78 | 16 | 32 |
| **MC-2** | T | 9.97 | 61 | 54 | 61 | 56 | 55 | 30 | 46 |
| | | 18.87 | 33 | 45 | 33 | 48 | 46 | 13 | 27 |
| | C | 9.97 | 54 | 60 | 54 | 62 | 61 | 27 | 40 |
| | | 18.87 | 74 | 76 | 74 | 77 | 77 | 25 | 36 |
| | B | 9.97 | 42 | 50 | 42 | 51 | 50 | 19 | 37 |
| | | 18.87 | 35 | 51 | 35 | 54 | 52 | 20 | 35 |
| **MC-3** | T | 9.97 | 77 | 66 | 77 | 69 | 67 | 16 | 32 |
| | | 18.16 | 70 | 58 | 70 | 59 | 59 | 19 | 30 |
| | C | 9.97 | 82 | 70 | 82 | 73 | 71 | 28 | 40 |
| | | 18.16 | 85 | 73 | 85 | 75 | 74 | 13 | 27 |
| | B | 9.97 | 86 | 72 | 86 | 73 | 72 | 29 | 42 |
| | | 18.16 | 72 | 61 | 72 | 62 | 62 | 25 | 35 |

The threshold value for Kittler-Illingworth and Otsu methods were equal for all images analyzed. The value for the ACWE, Niblack and Ridler-Calvard were similar, with maximum variance of three units. The Manual method provided a smaller threshold for all images when compared with the automated segmentation.

For the plug MC-1 the images with the pixel size of 9.97µm presented the threshold values higher than the images with pixel size of 16.03µm when using the Manual method. For the other methods, the threshold values were lower for the images with the pixel size of 9.97μm.

For the plugs MC-2 and MC-3, the images with the pixel size of 9.97μm presented the threshold values higher than the images with pixel size of 18.87μm when using the Manual method. For the other methods, central images with the pixel size of 9.97μm had a lower threshold value than the images with pixel size of 18.87μm and, most of the time, on the top and bottom images the threshold values were higher.

It was possible to calculate the porosity of each image using its respective threshold value obtained with the segmentation methods. The porosity values are shown in Table 3. The result of the porosity calculated with the Manual method is the sum of the macroporosity and microporosity calculated as Vidal & Soares (2015) suggested.

Table 3. Porosity value of each image (T-top, C-central, B-bottom) calculated with threshold obtained with six different segmentation methods of three samples from Morro do Chaves Formation.

| **Sample** | | **Pixel Size (μm)** | **Digital Porosity (%)** | | | | | |
|---|---|---|---|---|---|---|---|---|
| | | | Kittler & Illingworth | Ridler & Calvard | Otsu | ACWE | Niblack | Manual |
| **MC-1** | T | 9.97 | 18 | 13 | 18 | 13 | 13 | 10 |
| | | 16.03 | 15 | 13 | 15 | 14 | 13 | 2 |
| | C | 9.97 | 19 | 17 | 19 | 18 | 17 | 7 |
| | | 16.03 | 17 | 14 | 17 | 15 | 14 | 5 |
| | B | 9.97 | 20 | 14 | 20 | 15 | 14 | 8 |
| | | 16.03 | 20 | 14 | 20 | 14 | 14 | 4 |
| **MC-2** | T | 9.97 | 19 | 15 | 19 | 16 | 15 | 9 |
| | | 18.87 | 12 | 19 | 12 | 22 | 20 | 8 |
| | C | 9.97 | 14 | 17 | 14 | 19 | 18 | 7 |
| | | 18.87 | 16 | 17 | 16 | 18 | 18 | 2 |
| | B | 9.97 | 12 | 18 | 12 | 19 | 19 | 6 |
| | | 18.87 | 9 | 18 | 9 | 12 | 19 | 6 |
| **MC-3** | T | 9.97 | 19 | 15 | 19 | 16 | 16 | 8 |
| | | 18.16 | 19 | 14 | 19 | 14 | 14 | 7 |
| | C | 9.97 | 19 | 15 | 19 | 16 | 16 | 9 |
| | | 18.16 | 16 | 11 | 16 | 12 | 11 | 3 |
| | B | 9.97 | 20 | 16 | 20 | 16 | 16 | 9 |
| | | 18.16 | 17 | 12 | 17 | 12 | 12 | 5 |

The porosity obtained using the Kittler-Illingworth and Otsu methods were equal for all images. The results were similar for the ACWE, Niblack and Ridler-Calvard methods, and the porosity calculated with the Manual method was different from the results of the other methods.

In all images of the samples MC-1 and MC-3, the porosity calculated with Kittler-Illingworth and Otsu methods were the highest when compared to the other methods. The sample MC-2, different from the other two, presented the highest porosity values correlated with the other methods, except for the top image from plug MC-2, that had the highest porosity value when segmented with the Kittler-Illingworth and Otsu methods. The porosity values calculated with the Manual method were the lowest for all samples.

The porosity variation of the images in the same plug was relatively small and did not exceed 7%. For the images with pixel size of 9.97µm, the smallest variation was 0% and 1% for MC-3 independent of the method used. On the other hand, the highest variation was 6% and 7% for the MC-2 when segmented with the automated methods. For the samples with pixel size around 18µm, the smallest variation was 1% on MC-1 when segmented with the ACWE, Niblack and Ridler-Calvard methods. The highest variation was 6% on MC-2 segmented with the Manual method.

It was possible to calculate the variation of the threshold value between the three images of its respective plug. Analyzing the images with pixel size of 9.97µm, for MC-1 the variation was approximately 5% for Kittler-Illingworth and Otsu methods, 11% for ACWE, Niblack and Ridler-Calvard methods, and 4% for Manual method. To MC-2 the variation was 7% for Kittler-Illingworth and Otsu methods and 4% for the other four methods. To MC-3 the variation was 4% for Kittler-Illingworth, Otsu and Manual methods, 2% for the other three methods. On the other hand, when analyzing the images with pixel size of approximately 18µm, the variation was around 7% for the Kittler-Illingworth and Otsu methods, 9% for ACWE, Niblack and Ridler-Calvard methods, and 5% for the Manual method for MC-1. To MC-2, the variation was 16% for the Kittler-Illingworth and Otsu methods, 12% for the other four methods. For the sample MC-3, the variation was 6% for the Kittler-Illingworth, Otsu, ACWE, Niblack and Ridler-Calvard methods, and 4% for the Manual method.

The arithmetic mean of the threshold values was calculated for the top, central and bottom images of each plug for each method. The result, shown in Table 4, was used to segment the stacked images of the rock plugs and to calculate the total porosity of each sample (Figure 6). The VOI used for the calculation of the porosity was approximately 12cm³, 16cm³ and 2cm³ for samples MC-1, MC-2 and MC-3, respectively. The final porosity value obtained for each method is in Table 5. The result was compared with the values acquired with the helium porosimeter, which is considered the most accurate procedure to measure the porosity of rocks (Lucia, 2007).

Table 4. Arithmetic mean of the threshold value of the top, central and bottom images calculated from three images of MC-1, MC-2, MC-3 plugs, from Morro do Chaves Formation, using six different segmentation methods.

| **Sample** | **Pixel Size (µm)** | **Methods - Threshold** | | | | | | |
|---|---|---|---|---|---|---|---|---|
| | | Kittler-Illingworth | Ridler-Calvard | Otsu | ACWE | Niblack | Manual Porosity | |
| | | | | | | | Macro | Micro |
| **MC-1** | 9.97 | 80 | 71 | 80 | 72 | 71 | 37 | 55 |
| | 16.03 | 101 | 92 | 101 | 94 | 93 | 28 | 45 |
| **MC-2** | 9.97 | 52 | 55 | 52 | 56 | 56 | 25 | 41 |
| | 18.87 | 47 | 57 | 47 | 60 | 58 | 19 | 33 |
| **MC-3** | 9.97 | 82 | 69 | 82 | 72 | 70 | 24 | 38 |
| | 18.16 | 76 | 64 | 76 | 65 | 65 | 19 | 31 |

When comparing the porosity obtained from the VOI of the µCT images with two different pixel sizes, it can be seen that in samples MC-2 and MC-3 the porosity value was higher for the images with pixel size of 9.97µm in all segmentation methods. For the MC-1, the two resolutions obtained the same porosity results.

The segmentation methods that resulted in a higher porosity for the VOI were Kittler-Illingworth and Otsu for the plugs MC-1 and MC-3 with both pixel size images. For the MC-2 plug, the highest porosity value was acquired with the segmentation algorithms of Niblack and ACWE (Figure 7).

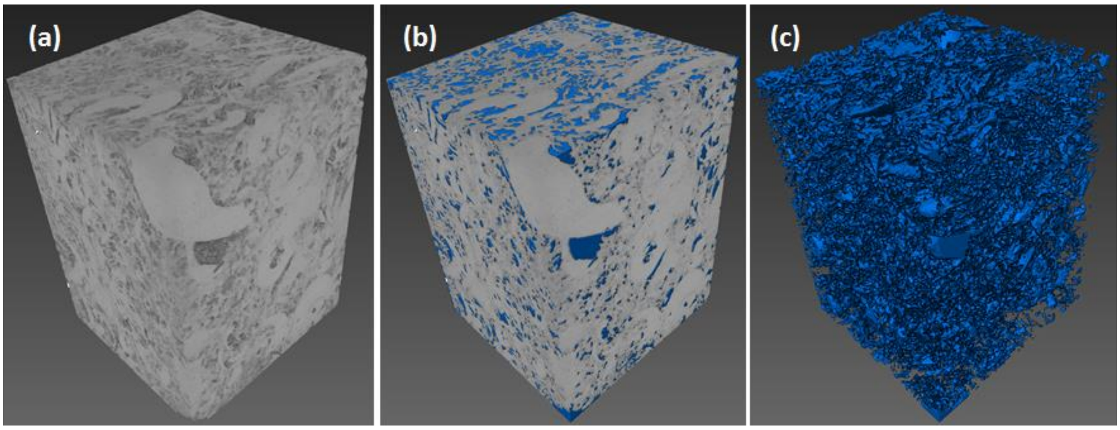


Figure 6. Extraction of the porous system of plug MC-2 with pixel size of 18.87μm. The porous system was extracted from a cuboid obtained from the stacked images. (a) Cuboid with non-local means filter; (b) overlap between binarized image with Niblack method, with a threshold value of 58, and the rock volume; (c) total porous system generated from the threshold value obtained by the Niblack method.

Table 5. Porosity value for the plugs MC-1, MC-2 and MC-3, from Morro do Chaves Formation, calculated using the arithmetic mean of threshold value obtained from the top, central and bottom image of them through six segmentation methods.

| **Sample** | **Helium porosity (%)** | **Pixel Size (μm)** | **Digital Porosity of the VOI (%)** | | | | | |
|---|---|---|---|---|---|---|---|---|
| | | | Kittler-Illingworth | Ridler-Calvard | Otsu | ACWE | Niblack | Manual |
| **MC-1** | 18 | 9.97 | 17 | 13 | 17 | 14 | 13 | 7 |
| | | 16.03 | 17 | 13 | 17 | 14 | 13 | 3 |
| **MC-2** | 20 | 9.97 | 13 | 15 | 13 | 16 | 16 | 6 |
| | | 18.87 | 6 | 8 | 6 | 10 | 9 | 2 |
| **MC-3** | 16 | 9.97 | 23 | 17 | 23 | 18 | 18 | 9 |
| | | 18.16 | 13 | 10 | 13 | 10 | 10 | 4 |

The highest porosity result in the VOI also meant a greater proximity to the Helium porosity for both MC-1 and MC-2 samples and resolutions and MC-3 with pixel size of 18μm. However, it was not the same for MC-3 with pixel size of 9.97μm. In this case, the Ridler-Calvard method resulted in porosity closer to that of the helium porosimeter.

When the porosity values obtained through μCT were compared with those of the helium porosimeter, it was observed that the images with smaller pixel size approximate more with the experimental result. For the images with pixel size of 9.97μ the difference was -1%, -4% and + 1% for MC-1, MC-2 and MC-3 respectively. For the images with pixel size of 18μm the difference was -1%, -10% and -3% for MC-1, MC-2 and MC-3, respectively.

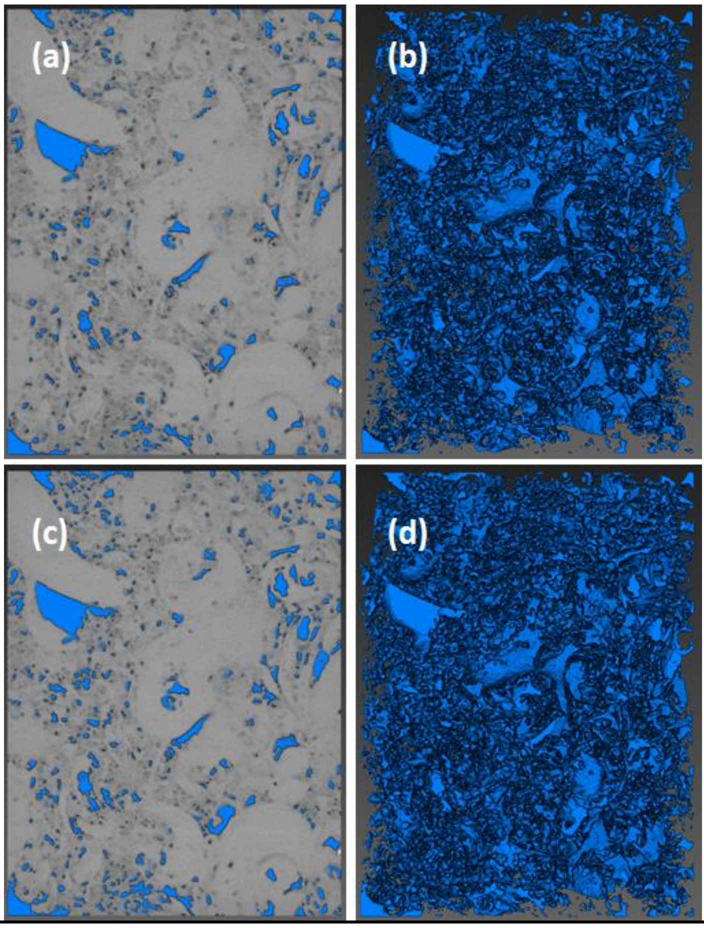


Figure 7. Comparison between the porous system obtained by two different segmentation methods, from the μCT images of plug MC-2 with pixel size of 18.87μm: (a) overlap between the rock volume and the porous system obtained by Kittler-Illingworth method; (b) the porous system generated with the threshold 47 obtained by Kittler-Illingworth method; (c) overlap between the rock volume and the porous system obtained by Niblack method; (d) the porous system generated with the threshold 58 obtained by Niblack method.

## 5. CONCLUSION AND DISCUSSION

The porosity of three samples of coquinas from Morro do Chaves Formation was analyzed with six segmentation methods using μCT images with two pixel sizes, 10μm and 18μm approximately. The methods used were Kittler-Illingworth, Ridler-Calvard, Otsu, ACWE, Niblack and Manual.

The μCT images with better resolution, in other words with smaller pixel size value, presented better porosity results when segmented. Although the acquisition and reconstruction process were more time consuming for those images, the results were worth the extra time. The difference between the results acquired with the segmentation methods and with the helium porosimeter were ±1% for the images with pixel size of 9.97μm and -3% to -10% for the images with pixel size approximately of 18μm.

For the samples studied, the segmentation method that most matched the helium porosity was Kittler-Illingworth and Otsu methods for samples MC-1 and MC-2. As for MC-3, the best method was the ACWE. Notwithstanding, this method took a considered amount of time to be analyzed. Thus, it can be considered that the best methods of segmentation for these coquinas were the Kittler-Illingworth and Otsu, which generated satisfactory results in a short period of time.

Although the automated segmentation methods gave a more satisfactory porosity result, they did not represent very well the porous media. The methods with algorithms used in this study had difficulty distinguishing small pores that were very close to each other and recognized them as one (Figure 3). That is, the automated methods considered some rock regions as pore. A solution would be to use the automatic method, but with the critical analysis of a specialist to identify if the pore space is well represented, changing the threshold value if necessary. Thus, the porous system would be more accurately represented, once the operator can distinguish pore from rock in an efficient way.

The variation of porosity from region to region within these carbonates means that comparison with a bulk measurement such as plug porosity will always present challenges. The automation is attractive when many samples have to be treated but the role of the expert operator might be difficult to eliminate, even for a single carbonate rock system.

For further researches, the same study can be performed with a larger range of samples, using codes that accept the µCT images stacked. One should also cut the images in a cylindrical format, so that it is not necessary to crop them in rectangular shapes, trying to obtain the maximum region and volume. This is an important process to be done, once the threshold value and, consequently, the porosity, can vary depending on the cut done in the image.

***Acknowledgements***

The authors would like to acknowledge funding from Shell, Petrobras, ANP, CNPq and CAPES. We thank LRAP, LAGESED and LIN teams in UFRJ for their support. We also would like to thank Professor Ricardo Tadeu, for the use of the µCT equipment SkyScan1173 for this research; and SACL project (Lagesed-UFRJ/Coppetec/BG E&P Brazil) for the availability of the samples.

## REFERENCES

Al-Raoush, R. I., & Willson, C. S., 2005. A pore-scale investigation of a multiphase porous media system. *Journal of Contaminant Hydrology*, vol. 77, n. 1, pp. 67-89.

Chan, T. F., Vese, L. A., 2001. Active Contours without Edges. *IEEE Transactions on Image Processing*, vol. 10, n. 2, pp. 266-277.

Corbett, P. W. M., Wang, H., Camara, R. N., Tavares, A-C., Borghi L. F. A., Perosi, F., Machado, A., Jiang, Z., Ma, J., , Bagueira, R., 2017. Using the Porosity Exponent (m) and Pore-Scale Resistivity Modelling to Understand Pore Fabric Types in Coquinas (Barremian-Aptian) of the Morro do Chaves Formation, NE Brazil. *Marine and Petroleum Geology*, Accepted for publication

Corbett, P. W. M.; Estrella, R.; Rodriguez, A. M.; Shoeir, A.; Borghi, L.; Tavares, A. C., 2016. Integration of cretaceous Morro do Chaves rock properties (NE Brazil) with the Holocene Hamelin coquina architecture (Shark Bay, Western Australia) to model effective permeability. *Petroleum Geoscience*, vol. 22, n. 2, pp. 105-122,

Corbett, P. W. M. & Borghi, L., 2013. Lacustrine carbonates – for the purpose of reservoir characterization are they different?. *Offshore Technology Conference*, 29–31 October 2013, Rio de Janeiro, Brazil.

Dias, L.O., De Bom, C.R., Guimarães, H., Faria, E.L., Márcio, P., Marcelo, P., Correia, M.D. and Surmas, R., 2016. Segmentação textural de imagens de rocha por microtomografia

Segmentation of microtomography images of rocks using texture filter. *Notas Técnicas*, vol. 6, n. 1.

Estrella, R., 2015. Variação da porosidade e da permeabilidade em coquinas da Formação Morro do Chaves (andar Jiquiá), Bacia de Sergipe-Alagoas. Undergraduate Thesis, Universidade Federal do Rio de Janeiro.

Iassonov, P., Gebrenegus, T. and Tuller, M., 2009. Segmentation of X-ray computed tomography images of porous materials: A crucial step for characterization and quantitative analysis of pore structures. *Water Resources Research*, vol. 45, n. 9.

Kittler, J., & Illingworth, J., 1986. Minimum error thresholding. *Pattern recognition*, vol. 19, n. 1, pp. 41-47.

Lucia, F. J., 2007. Carbonate reservoir characterization: an integrated approach. *Springer Science & Business Media*.

Neto, J. M. R., Fiori, A. P., Lopes, A. P., Marchese, C., Pinto-Coelho, C. V., Vasconcellos, E. M. G., Silva, G. F., Secchi, R., 2011. A microtomografia computadorizada de raios x integrada à petrografia no estudo tridimensional de porosidade em rochas. *Revista Brasileira de Geociências*, vol. 41, n. 3, pp. 498-508.

Niblack W., 1986. An introduction to image processing. *Prentice-Hall, Englewood Cliffs*, pp. 115–116.

Otsu, N., 1979. A threshold selection method from gray-level histograms. *IEEE transactions on systems, man, and cybernetics*, vol. 9, n. 1, pp. 62-66.

Ridler, T.W., & Calvard, S., 1978. Picture thresholding using an iterative selection method. *IEEE transactions on systems, man, and cybernetics*, vol. 8, n. 8, pp. 630-632.

Sezgin, M., & Sankur, B., 2004. Survey over image thresholding techniques and quantitative performance evaluation. *Journal of Electronic Imaging*, vol. 13, n. 1, pp. 146–165.

Silva, W. G. A. L., 2015. Análise do espaço poroso para simulação numérica do escoamento de fluidos em estromatólito utilizando microtomografia computadorizada de raios X. Master thesis, COPPE, Universidade Federal do Rio de Janeiro.

Vidal, A. D., Soares, J. A., 2015. Quantificação da macro e micro porosidade e sua conectividade em rochas carbonáticas por microtomografia de raios X. Undergraduate Thesis, Universidade Federal de Campina Grande.

Wildenschild, D., Vaz, C. M. P., Rivers, M. L., Rikard, D., Christensen, B. S. B., 2002. Using X-ray Computed Tomography in Hydrology: Systems, Resolutions, and Limitations. *Journal of Hydrology*, vol. 267, n. 3, pp. 285-297.